

Dynamic Exercise Imaging With an MR-Compatible Stationary Cycle Within the General Electric Open Magnet

Christopher P. Cheng,¹ Douglas F. Schwandt,² Eric L. Topp,² James H. Anderson,² Robert J. Herfkens,³ and Charles A. Taylor^{1,4*}

Many cases of muscular ischemia do not manifest without increased metabolic demand. Hence, diagnosis of intermittent claudication often requires inducing physiologic challenge, such as by exercise. Cine phase-contrast MRI can concurrently acquire cross-sectional vascular anatomy and through-plane blood velocities, enabling blood flow rate quantification. An MR-compatible stationary cycle was designed, constructed, and tested for flow quantification in large arteries during lower-limb exercise in a General Electric Signa SP 0.5 T open magnet. The cycle demonstrated smooth cycling during image acquisition, has freewheeling capability, is adjustable for subject size and strength, and can quantify workload. A healthy 59-year-old male was imaged at the supraceliac and infrarenal levels of the abdominal aorta at rest and during exercise. An exercise workload of 47.9 W was achieved. His heart rate increased from 52 to 78 bpm, supraceliac flow increased from 1.7 to 3.7 L/min, and infrarenal flow increased from 0.4 to 3.2 L/min from rest to exercise. Magn Reson Med 49:581–585, 2003. © 2003 Wiley-Liss, Inc. Key words: blood flow; exercise; functional flow imaging; lower-limb ischemia; abdominal aorta

Except for the most advanced states of disease, muscular ischemia only becomes evident during conditions of increased metabolic demand. For this reason, there are diagnostic and assessment techniques that involve approximating the physiologic challenges that patients may experience in daily life. These techniques include inducing exercise stress by treadmill walking, reactive hyperemia, and pharmacologic stress. While the patients are in these stressed states, diagnoses are made based on Doppler ultrasound, nuclear imaging, segmental arterial pressures, and muscle pain. While these indicators can be used to infer blood flow rate, they do not measure volume flow and are prone to inaccurate assessments.

In the field of vascular disease research, dynamic exercise flow studies are also essential in order to understand the physiologic effects that these stress conditions have on the body. For instance, understanding the mechanisms by

which exercise contributes to the prevention and regression of cardiovascular disease may potentially improve therapies. Exercise, in combination with smoking cessation, is the most consistent treatment for ischemia in the lower extremities (1). It is hypothesized that these benefits of exercise are related to biologic phenomena that result, at least in part, from hemodynamic alterations in the major vessels (2–6). Specifically, exercise has been shown to increase low flow rate and low wall shear stress, and decrease oscillations in flow in the infrarenal abdominal aorta, which are observed at rest (7–9).

Phase contrast magnetic resonance imaging (PC-MRI) can concurrently acquire high-resolution, coregistered, through-plane velocity and anatomic maps. This allows the segmentation of large vessel lumens, and quantification of temporally-resolved volume flow rate through integration of blood velocities over the lumen (10). Spatially- and temporally-resolved wall shear stress values can also be quantified by computing velocity gradients in the vicinity of the lumen wall (11).

Due to space and material compatibility constraints, most prior nonbasal MRI analyses have been restricted to motionless states, such as during postprandial (12), pharmacologically-induced (13–15), and exercise-recovery (8) conditions. While these studies have improved our understanding of many nonbasal states, dynamic exercise is an important functional state to investigate for the reasons explained above. With conventional MRI, measurements have been restricted to rest and very mild exercise conditions due to the movement-limiting space constraints in conventional MRI bores (8,16). In addition, these exercise states can only be performed in a supine position. However, with a 0.5T open magnet (General Electric Signa SP, General Electric Medical Systems, Milwaukee, WI), a subject can sit upright in the bore and pedal an MR-compatible stationary cycle to achieve higher levels of exercise in a more natural exercise posture (9). We have built an MR-compatible cycle for the General Electric open magnet to measure blood flow velocity in the abdominal aorta of upright subjects during rest and exercise conditions *in vivo*. This novel design enables smooth actuation, durability, and adjustability for patient size and strength, and offers the ability to vary and quantify exercise workload, ensuring repeatable exercise intensities for intra- and intersubject studies.

METHODS

The functional requirements of our MR-compatible cycle were: 1) limited abdomen motion during exercise to min-

¹Department of Mechanical Engineering, Stanford University, Stanford, California.

²Veterans Affairs Palo Alto Rehabilitation Research and Development Center, Palo Alto, California.

³Department of Radiology, Stanford University, Stanford, California.

⁴Department of Surgery, Stanford University, Stanford, California.

Grant sponsor: NIH; Grant number: P41RR09784; Grant sponsors: Lucas Foundation; Whitaker Foundation.

*Correspondence to: Charles A. Taylor, Division of Biomechanical Engineering, Durand Building, Room 213, Stanford, CA 94305-3030. E-mail: taylorca@stanford.edu

Received 19 July 2002; revised 7 October 2002; accepted 7 October 2002.

DOI 10.1002/mrm.10364

Published online in Wiley InterScience (www.interscience.wiley.com).

© 2003 Wiley-Liss, Inc.

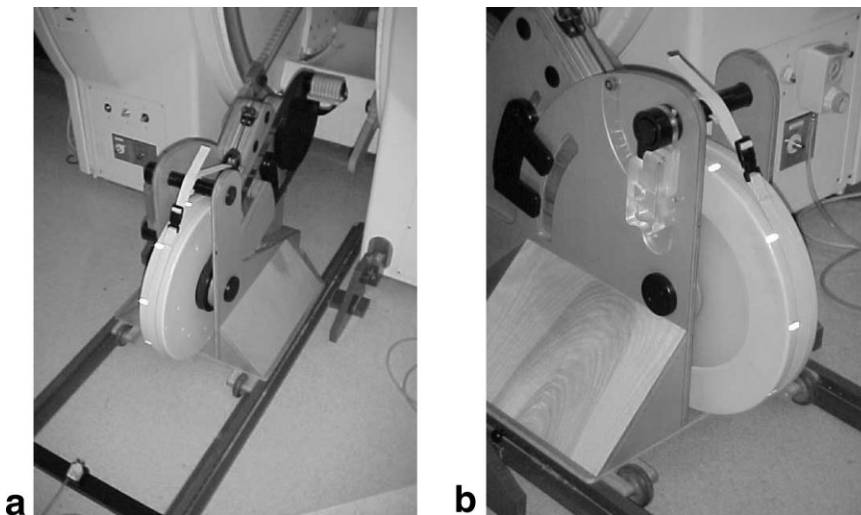


FIG. 1. Photographs of the MR-compatible cycle as it is bolted into the GE 0.5T open magnet. **a:** Right view of the cycle shows the pedal sprocket that actuates the flywheel by a Kevlar-reinforced timing belt. The white strap provides friction on the flywheel, which acts as the load against pedaling. **b:** Left view shows the pendulum whose deflection corresponds to the flywheel friction force. The product of the torque required to drive the flywheel, and the angular speed of the flywheel, measured by the light sensor (bottom left of image **a**) counting the passing reflective markers on the flywheel, is equal to the instantaneous workload.

imize motion-induced blurring, 2) variable resistance to accommodate for variations in subject strength, 3) freewheeling capability to avoid forced leg motion after the onset of pain in claudication patients, 4) adjustability for subject size, and 5) instrumentation for mechanical work measurement for intra- and intersubject comparisons.

The cycle features seven major design elements: 1) MR compatibility, 2) crank tower, 3) power transmission system, 4) freewheel mechanism, 5) load generation and measurement, 6) cycle supports and guide rails, and 7) workload acquisition system. Left and right views of the completed cycle are shown in Fig. 1. Each of these design elements is described in more detail below.

- 1) MR compatibility. We avoided ferrous materials and limited the use of nonferrous metals to very small components that are located far away from the bore of the magnet. Most of the cycle is made from Delrin[®] plastic and birch plywood.
- 2) Crank tower. The crank tower pivots about the flywheel center through a range of angles and can be locked in place with quick-release clamps, enabling height adjustment. The pedal shafts attach to the cranks, and the cranks to the crank shaft, with mating hexagonal tapers secured by a bolt, all made from Delrin[®]. This provides secure mechanical engagement specifically designed for transmitting pedaling loads.
- 3) Power transmission system. A crank sprocket roughly 33 cm in diameter drives a smaller flywheel sprocket with a 2:1 gear ratio. A Kevlar-reinforced cogged timing belt connects the two sprockets.
- 4) Freewheel mechanism. The flywheel is driven by a roller-clutch silent freewheeling mechanism built into the flywheel sprocket. Small brass rollers in spiral grooves engage a drive ring on the flywheel when driven forward, transmitting pedaling torques to the flywheel. The rollers disengage when the cycle is driven backward or the subject stops pedaling, thereby allowing freewheeling.
- 5) Load generation and measurement. Pedaling torque is resisted by the frictional torque generated by a

cotton strap wrapped around a flat groove on the flywheel, similar to a prony brake mechanism. A tensioning pulley with an elastic cord controls the strap friction on the flywheel, while the strap is connected to a shaft that drives a free-hanging pendulum. The friction force that causes deflection in the pendulum is exactly the force that drives the flywheel, similar to the design of the Monark pendulum balance ergometer (Monark Exercise AB, Vansbro, Sweden). The full-scale pendulum torque may be adjusted incrementally for higher work loads by attaching calibrated weights to the pendulum.

- 6) Supports and guide rails. Supports provide stability for the cycle during exercise and horizontal adjustability for subject size. Height adjustment is achieved by pivoting the crank tower up and down, while the distance from the seat is adjusted by changing where the cycle is attached along two guide rails, which are bolted to the MR open magnet.
- 7) Workload acquisition. The product of the angular velocity of the wheel (ω) and the sum of the system friction torque (FT) plus flywheel torque (τ) is equal to the mechanical workload, as described in the equation: $\text{workload} = \omega \times (\text{FT} + \tau)$. The angular velocity is calculated by counting passing reflective markers placed around the circumference of the spinning flywheel with a stationary photosensor (MiniBEAM SM312LV; Banner Engineering Corp., Minneapolis, MN). This information is transmitted outside of the MR room through a penetration panel and acquired using an A/D acquisition board (DAQPad-6020E; National Instruments, Austin, TX) and LabVIEW (National Instruments, Austin, TX). The flywheel torque is computed from the deflection of the pendulum.

In order to demonstrate the effectiveness of the MR-compatible stationary cycle described above, a single male subject was imaged at rest and during steady-state lower-limb exercise at the supraceliac and infrarenal levels of the aorta using cine PC-MRI in a General Electric open magnet (main field = 0.5 T, gradient strength = 1.2 Gauss/cm, slew rate = 12 Gauss/cm/ms) with a General Electric trans-

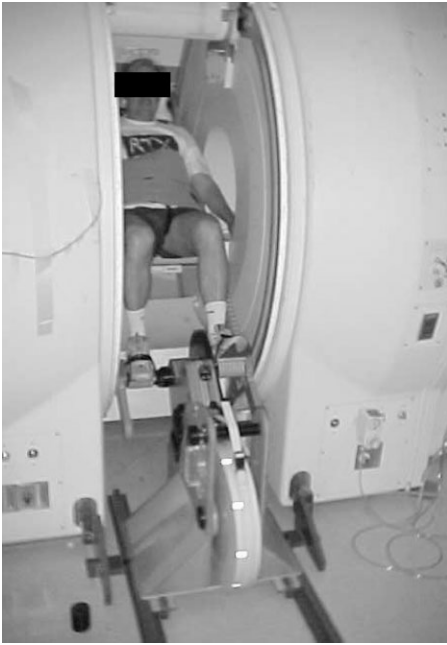


FIG. 2. Image acquired while the MR-compatible stationary cycle was pedaled in the GE Signa SP 0.5T open magnet.

mit/receive body surface coil. The subject breathed normally during the acquisitions, and respiratory bellows were used to perform respiratory compensation (17). The scan parameters included: TR = 25 ms, TE = 9 ms, flip angle = 30°, slice thickness = 10 mm, square field of view (FOV) = 26 × 26 cm, matrix = 256 × 128, and velocity-encoding gradient = 150 cm/s. The cine acquisitions were gated to the cardiac cycle using a plethysmograph placed on the right thumb, and data collected over 256 heartbeats were retrospectively reconstructed to 16 time points within the cardiac cycle. From the imaging data, blood flow rate was computed by segmentation of the aortic lumen by level-set segmentation of the magnitude data (18), adjustment of the phase data with a second-order baseline correction (19), and integration of blood flow velocities within the cross section of the lumen to calculate volume flow rate (10). The imaging protocol was approved by the Stanford University Panel on Human Subjects in Medical Research.

RESULTS

The MR-compatible cycle actuates smoothly and the system friction remains constant for extended periods of cycling. The dynamic torque required to drive the flywheel without any strap friction load is 0.682 Nm. Installation and operation was smooth in the open magnet and image quality was not affected. Figure 2 shows the MR-compatible cycle as it connects to the 0.5 T open magnet with a subject pedaling during image acquisition. The subject (male, age 59) increased his resting heart rate of 52 bpm to a steady-state exercise heart rate of 78 bpm. The steady-state workload was calculated to be 47.9 W by the equation:

$$\text{Angular velocity: } \omega = 15.71 \text{ rad/s}$$

$$\text{System Friction torque: } FT = 0.682 \text{ Nm}$$

$$\text{Flywheel torque: } \tau = 2.36 \text{ Nm}$$

$$\text{Workload} = \omega \times (FT + \tau) = 47.9 \text{ Watts} . \quad [1]$$

Flow rates and blood velocities for the supraceliac and infrarenal levels of the aorta at rest and during lower limb exercise are shown in Fig. 3. At the supraceliac level, the mean flow rate increased from 1.7 L/min at rest to 3.7 L/min during exercise, and at the infrarenal level increased from 0.4 L/min at rest to 3.2 L/min during exercise. At the infrarenal location, reversal of flow was observed during diastole at rest, but the flow increased and became unidirectional for the cardiac cycle during exercise.

DISCUSSION

As stated in Methods, ferrous metals were avoided and nonferrous metals were kept to a minimum. At the rotating joints, including the two pedal shafts, crank shaft, flywheel shaft, and workload pendulum shaft, stainless steel full-complement needle or ball bearings are used to reduce friction and extend joint lifespan. Plastic bearings were replaced with these bearings due to excessive heat generation and eventual joint seizure. Brass dowel pins were used for the roller-clutch freewheeling mechanism because plastic pins deformed over time and caused the freewheel to slip on the flywheel sprocket. These components are very small and are at least 4 feet away from the center of the magnet bore during operation. There are also two stationary nonferrous metal components, including a small stainless steel spring in the cam cleat that grips the tensioning cord (for adjusting flywheel friction), and the bolts that fasten the rails to the base of the open magnet. These components were not magnetically attracted toward the magnet, nor did they create any perceptible imaging artifacts.

This study shows that the MR-compatible cycle described herein is capable of producing smooth, repeatable lower-limb exercise while cine PC-MRI is performed in the abdominal aorta. A 50% increase in resting heart rate was easily achieved, and the mechanical workload was quantifiable. The blood flow results we quantified in this study compare favorably with previous functional flow imaging studies in the human abdominal aorta (7–9,16). From rest to exercise, mean flow rates in the aorta increased, volume flow waveforms transitioned from triphasic to biphasic, infrarenal flow reversal was eliminated, and digestive and renal flow decreased (1.3 L/min at rest to 0.5 L/min during exercise).

Combined with PC-MRI techniques, imaging during states of exercise challenge can be a valuable tool for diagnosing lower-extremity occlusive disease, planning treatments preoperatively, assessing treatments, and predicting intervention patency. For example, a subnormal increase in blood flow due to exercise could indicate hemodynamically significant stenoses in the vasculature,

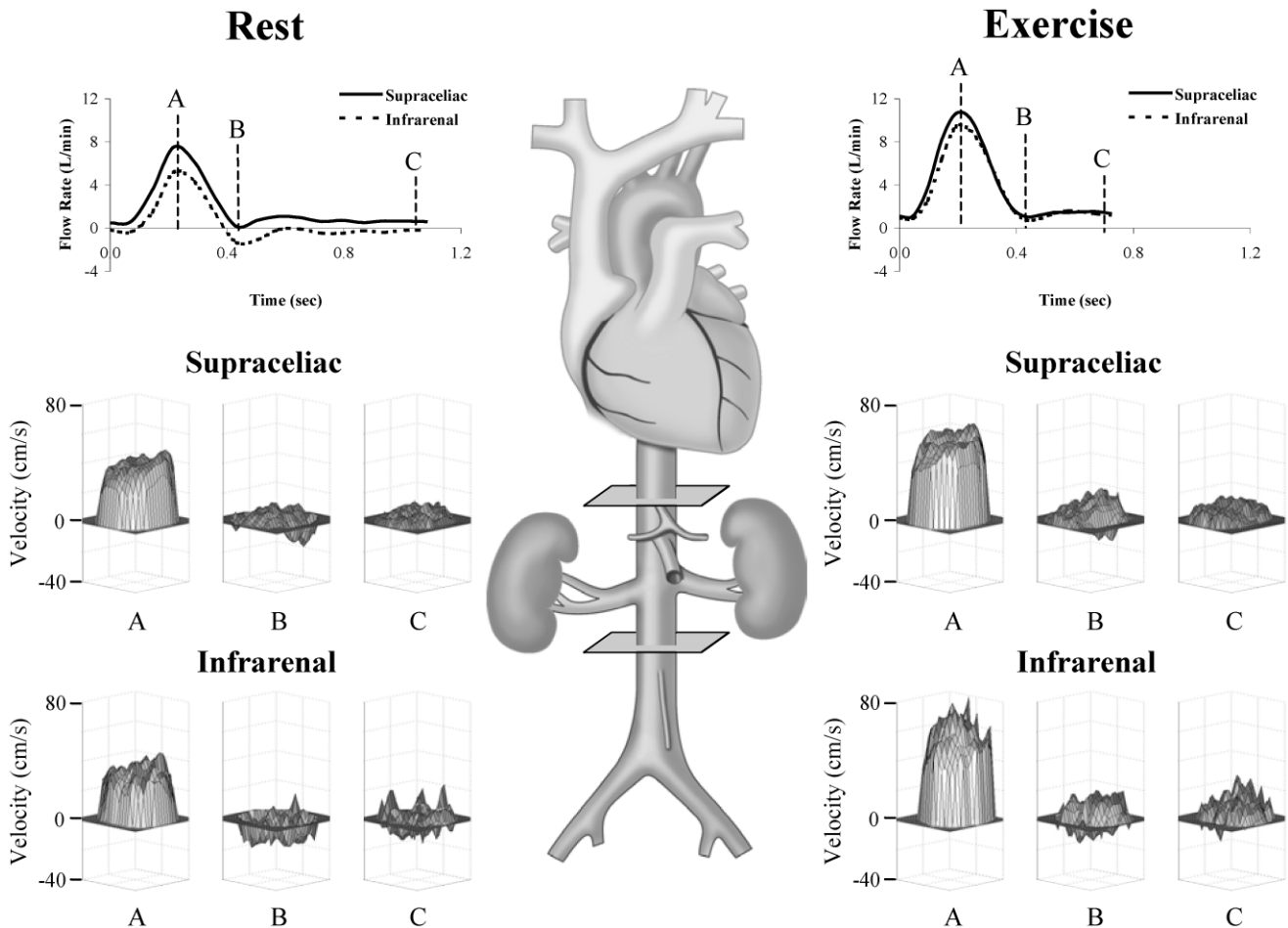


FIG. 3. Drawing of the human aorta with imaging planes at the supraceliac and infrarenal levels. Blood flow rate waveforms (top of figure) show significant increases in flow at both the supraceliac and infrarenal levels from rest (left) to exercise (right) throughout the cardiac cycle. Also note that reversal of flow at the infrarenal level at rest is eliminated during exercise. Velocity surface plots are shown for the supraceliac (middle) and infrarenal (bottom) levels of the aorta at rest (left) and during exercise (right) at (A) peak systole, (B) end systole, and (C) end diastole. Blood velocities increase from rest to exercise for all cardiac phases, and in the infrarenal aorta, negative velocities near the wall at (b) end systole at rest (left) become positive during exercise (right).

while an increase in graft flow due to exercise could indicate a longer period of graft patency with postoperative physical activity. Also, the diameter of a bypass graft could be chosen to ensure adequate blood flow corresponding to a certain level of exercise intensity. While the current system is unable to target specific limbs or muscle groups because of leg motion and long imaging times (~ 2 min during exercise), the application of fast cine methods would allow localized imaging immediately postexercise (8) in an upright position. Furthermore, with the development of methods capable of image acquisition gated to both heart rate and cyclic leg motion, flow imaging could be targeted to the moving limbs.

These techniques will also aid in experimental investigations into the mechanisms by which exercise improves cardiovascular health. Comparison of the abdominal aortic hemodynamic environments of young and older normal subjects could reveal differences in the alterations of flow due to lower-limb exercise between the two age groups. This could help determine whether there are more adverse

hemodynamic conditions in the abdominal aortas of the older population, which more prevalently experience atherosclerosis. The current conventional methods of hemodynamic assessment can not quantify changes in flow due to exercise; therefore, functional vascular imaging could play an important role in the management of arterial insufficiency.

ACKNOWLEDGMENTS

We acknowledge the contributions of Machiel Van der Loos and Monroe Postman from the Palo Alto Veterans Affairs Rehabilitation Research and Development Center, and David Miller, Robert Siston, and Kate Saul from the Department of Mechanical Engineering at Stanford University, for their work on the design and construction of an earlier prototype of the MR-compatible cycle. We also thank Claudia Cooper of Stanford Radiology for assistance with image acquisition. Christopher Cheng was supported by a Whitaker Foundation predoctoral fellowship.

REFERENCES

1. Weitz J, Byrne J, Clagett P, Farkouth M, Porter J, Sackett D, Standness E, Taylor L. Diagnosis and treatment of chronic arterial insufficiency of the lower extremities: a critical review. *Circulation* 1996;94:3026–3049.
2. Nobutaka I, Ramasamy S, Fukai T, Nerem R, Harrison DG. Shear stress modulates expression of Cu/ZN superoxide dismutase in human aortic endothelial cells. *Circ Res* 1996;79:32–37.
3. Sessa W, Pritchard K, Seydi N, Wang J, Hintze T. Chronic exercise in dogs increases coronary vascular nitric oxide production and endothelial cell nitric oxide synthase gene expression. *Circ Res* 1994;74:349–353.
4. Wang J, Wolin SM, Hintze HT. Chronic exercise enhances endothelium-mediated dilation of epicardial coronary artery in conscious dogs. *Circ Res* 1993;73:838–929.
5. Zarins CK, Bomberger RA, Glagov S. Local effects of stenoses: increased flow velocity inhibits atherogenesis. *Circulation* 1981;64(2 Pt 2):221–227.
6. Taylor CA, Hughes TJR, Zarins CK. Effect of exercise on hemodynamic conditions in the abdominal aorta. *J Vasc Surg* 1999;29:1077–1089.
7. Niezen R, Doornbos J, van der Wall EE, de Roos A. Measurement of aortic and pulmonary flow with MRI at rest and during physical exercise. *J Comput Assist Tomogr* 1998;22:194–201.
8. Pedersen E, Kozerke S, Ringgaard S, Scheidegger MB, Boesiger P. Quantitative abdominal aortic flow measurements at controlled levels of ergometer exercise. *Magn Reson Imaging* 1999;17:489–494.
9. Taylor CA, Cheng CP, Espinosa LA, Tang BT, Parker D, Herfkens RJ. In vivo quantification of blood flow and wall shear stress in the human abdominal aorta during lower limb exercise. *Ann Biomed Eng* 2002;30:402–408.
10. Pelc NJ, Sommer FG, Li KC, Brosnan TJ, Herfkens RJ, Enzmann DR. Quantitative magnetic resonance flow imaging. *Magn Reson Q* 1994;10:125–147.
11. Cheng CP, Parker D, Taylor CA. Quantification of wall shear stress in large blood vessels using Lagrangian interpolation functions with cine PC-MRI. *Ann Biomed Eng* 2002;30:1020–1032.
12. Li KC, Whitney WS, McDonnell CH, Fredrickson JO, Pelc NJ, Dalman RL, Jeffrey RB. Chronic mesenteric ischemia: evaluation with phase-contrast cine MR imaging. *Radiology* 1994;190:175–179.
13. Globits S, Blake L, Bourne M, Fujita N, Duerinckx A, Szolar D, Cheitlin M, Higgins CB. Assessment of hemodynamic effects of angiotensin-converting enzyme inhibitor therapy in chronic aortic regurgitation by using velocity-encoded cine magnetic resonance imaging. *Am Heart J* 1996;131:289–293.
14. Lorenz I, Kolbitsch C, Schocke M, Kremser C, Zschiegner F, Hinteregger M, Felber S, Hormann C, Benzer A. Low-dose remifentanyl increases regional cerebral blood flow and regional cerebral blood volume, but decreases regional mean transit time and regional cerebrovascular resistance in volunteers. *Br J Anaesth* 2000;85:199–204.
15. Tello R, Hartnell GG, Hill T, Volpe J, Finn JP, Cohen M. MR perfusion imaging of the kidney pre- and post-dipyridamole stress. *J Magn Reson Imaging* 1996;6:460–464.
16. Schalet B, Taylor C, Harris E, Herfkens R, Zarins C. Quantitative assessment of human aortic blood flow during exercise. *Surg Forum* 1997;48:359–362.
17. Fredrickson JO, Wegmuller H, Herfkens RJ, Pelc NJ. Simultaneous temporal resolution of cardiac and respiratory motion in MR imaging. *Radiology* 1995;195:169–175.
18. Wang KC. Level set methods for computational prototyping with application to hemodynamic modeling. Ph.D. dissertation, Stanford University, Stanford, CA, 2001.
19. Bernstein MA, Zhou XJ, Polzin JA, King KF, Ganin A, Pelc NJ, Glover GH. Concomitant gradient terms in phase contrast MR: analysis and correction. *Magn Reson Med* 1998;39:300–308.